11-8-2018

Constraints on aerosol nitrate photolysis as a potential source of HONO and NOx, Environmental Science and Technology

Paul S. Romer
University of California

Paul J. Woolridge
University of California

John D. Crounse
California Institute of Technology

Michelle J. Kim
California Institute of Technology

Paul O. Wennberg
California Institute of Technology

See next page for additional authors

Recommended Citation

Romer, P. S., P. J. Wooldridge, J. D. Crounse, M. Kim, P. O. Wennberg, J. E. Dibb, E. Scheuer, D. R. Blake, S. Meinardi, A. L. Brosius, A. B. Thames, D. O. Miller, W. H. Brune, and R. C. Cohen (2018), Constraints on aerosol nitrate photolysis as a potential source of HONO and NOx, Environmental Science and Technology, Article ASAP (web publication), DOI: 10.1021/acs.est.8b03861.

Environmental Processes

Constraints on aerosol nitrate photolysis as a potential source of HONO and NO

Paul Romer, Paul J. Wooldridge, John D. Crounse, Michelle J Kim, Paul O. Wennberg, Jack Dibb, Eric Scheuer, Donald R. Blake, Simone Meinardi, Alexandra L. Brosius, Alexander B. Thames, David O. Miller, William H. Brune, Samuel R. Hall, Thomas B. Ryerson, and Ronald Carl Carl Cohen

Environ. Sci. Technol., **Just Accepted Manuscript** • DOI: 10.1021/acs.est.8b03861 • Publication Date (Web): 08 Nov 2018

Constraints on aerosol nitrate photolysis as a potential source of HONO and NO_x

Paul S. Romer,[†] Paul J. Wooldridge,[†] John D. Crounse,[‡] Michelle J. Kim,[‡] Paul O. Wennberg,[‡,¶] Jack E. Dibb,[§] Eric Scheuer,[§] Donald R. Blake,[‖] Simone Meinardi,[‖] Alexandra L. Brosius,[⊥] Alexander B. Thames,[⊥] David O. Miller,[⊥] William H. Brune,[⊥] Samuel R. Hall,[#] Thomas B. Ryerson,[@] and Ronald C. Cohen[*,†,△]

†*Department of Chemistry, University of California Berkeley, Berkeley, CA 94720, USA*

‡*Division of Geological and Planetary Sciences, California Institute of Technology, Pasadena, CA 91125, USA*

¶*Division of Engineering and Applied Science, California Institute of Technology, Pasadena, CA 91125, USA*

§*Institute for the Study of Earth, Oceans, and Space, University of New Hampshire, Durham, NH 03824, USA*

‖*Department of Chemistry, University of California Irvine, Irvine, CA 92697, USA*

⊥*Department of Meteorology and Atmospheric Science, The Pennsylvania State University, University Park, PA 16802, USA*

#*Atmospheric Chemistry Observations and Modeling Laboratory, NCAR, Boulder, CO 80301, USA*

@*Chemical Sciences Division, NOAA Earth System Research Laboratory, Boulder, CO 80305, USA*

△*Department of Earth and Planetary Sciences, University of California Berkeley, Berkeley, CA 94720, USA*

E-mail: rccohen@berkeley.edu

Abstract

The concentration of nitrogen oxides (NO_x) plays a central role in controlling air quality. On a global scale, the primary sink of NO_x is oxidation to form HNO_3. Gas-phase HNO_3 photolyses slowly with a lifetime in the troposphere of 10 days or more. However, several recent studies examining HONO chemistry have proposed that particle-phase HNO_3 undergoes photolysis 10–300 times more rapidly than gas-phase HNO_3. We present here constraints on the rate of particle-phase HNO_3 photolysis based on observations of NO_x and HNO_3 collected over the Yellow Sea during the KORUS-AQ study in summer 2016. The fastest proposed photolysis rates are inconsistent with the observed NO_x to HNO_3 ratios. Negligible to moderate enhancements of the HNO_3 photolysis rate in particles, 1–30 times faster than in the gas phase, are most consistent with the observations. Small or moderate enhancement of particle-phase HNO_3 photolysis would not significantly affect the HNO_3 budget, but could help explain observations of HONO and NO_x in highly aged air.

Introduction

Nitrogen oxides ($NO_x \equiv NO + NO_2$) are a central component of atmospheric chemistry, affecting air quality, climate, and ecosystem health. The concentration of NO_x regulates the concentration of major atmospheric oxidants and controls the pathways of atmospheric oxidation. Accurate knowledge of the chemical sources and sinks of NO_x is therefore vital to understanding atmospheric oxidation and predicting how air quality will respond to changes in anthropogenic emissions or to changes in the global climate system.

On a global scale, the largest sink of NO_x is oxidation of NO_2 by OH to form HNO_3.[1] In the lower troposphere, gas-phase HNO_3 is removed by wet and dry deposition, with an overall lifetime of only a couple days. Chemical removal of gas-phase HNO_3 is much slower, with a lifetime to photolysis or oxidation by OH of 15–30 days in the troposphere.[2] In remote locations, even this slow rate can be relevant and act as an important source of NO_x.

HNO_3 can also partition into aerosols, forming inorganic particle-phase nitrate (NO_3^-). Dry deposition is slow for most particles, but particle-phase nitrate can be lost by wet deposition, or it can be lost by re-partitioning between phases as gas-phase HNO_3 is deposited.[3] Throughout this manuscript, we use HNO_3 to refer to the sum of gas-phase nitric acid and inorganic particle-phase nitrate.

Previous studies examining the chemical evolution of NO_x and HNO_3 in the absence of fresh emissions have found varying results. While Bertram et al.[4] and Neuman et al.[5] found good agreement between observations and models, several other studies reported elevated concentrations of NO_x that could not be explained with known chemistry.[6–8] To reconcile models and observations, multiple pathways for the conversion of HNO_3 into NO_x or HONO have been proposed, a process termed re-noxification. Various re-noxification pathways have been proposed in areas including the upper troposphere,[7–9] the marine boundary layer,[6,10–12] rural forests,[13,14] and areas of continental outflow.[15] Recently, several of these studies have suggested that HNO_3 is rapidly photolyzed in aerosols to form NO_2 or HONO, at a rate between 10 and 300 times faster than the rate of gas-phase HNO_3 photolysis,[10–12,15,16] and it is this process that we investigate here.

Most of the previous studies of this process were primarily focused on the potential for particle-phase nitrate photolysis to explain observations of HONO. To complement the approach of previous studies, we examine the consequences of rapid nitrate photolysis on concentrations of NO_x and HNO_3. Because HONO is itself rapidly lost by photolysis to produce NO, the effect of nitrate photolysis on NO_x chemistry does not depend on whether HONO or NO_x is the direct product. Past studies investigating aerosol nitrate photolysis have reported their results as an enhancement factor (EF), relating the rate of nitric acid photolysis in the particle phase to that in the gas-phase (Eq. 1), and we follow that convention here.

$$j_{p\mathrm{HNO_3}} = EF \cdot j_{g\mathrm{HNO_3}} \quad (1)$$

While mechanistic studies of aerosol nitrate photolysis are limited, investigations of pho-

tolysis in solution or on surfaces help explain how large enhancements of aerosol-phase nitrate photolysis could be possible. In solution, the cross section of NO_3^- is enhanced by a factor of 25 at 310 nm over that of gas-phase HNO_3, likely due to symmetry-breaking of the NO_3^- ion by hydration.[17] At the same time, the quantum yield of NO_3^- photolysis is reduced from near unity in the gas-phase to 0.01 in bulk solution, likely due to recombination of the photolysis products in the solvent cage, leading to an overall slower rate of aqueous-phase nitrate photolysis than that of gas-phase nitric acid.[18,19]

In contrast, nitric acid or nitrate adsorbed on surfaces is not fully enclosed in a solvent cage and is therefore expected to have an enhanced cross section without a significant decrease in the quantum yield. Experimental results have confirmed that the cross section of HNO_3 can be enhanced by up to a factor of 1000 at 308–310 nm when adsorbed onto the surface of aluminum or ice. The quantum yield of HNO_3 on the same surfaces was 0.60 or greater.[20,21] Thus, if a significant portion of aerosol nitrate is located on or near the aerosol surface, where its quantum yield remains high, then it is plausible that its photolysis rate could be enhanced multiple orders of magnitude over that of gas-phase nitric acid.

The ratio of NO_x to HNO_3, which we refer to as R_{obs}, provides crucial information about the chemistry of HNO_3. R_{obs} has been used in past studies to investigate both the production and loss of HNO_3.[5–9] As a ratio of two concentrations, R_{obs} is relatively unaffected by the total concentration of reactive nitrogen (NO_y) or the total volume of emissions encountered. By eliminating the effects of emissions and dilution, analysis of R_{obs}, rather than absolute HNO_3 concentration, helps isolate the effects of HNO_3 production and loss and allows comparison of airmasses between different environments.

In this paper, we present new constraints on the rate of particulate nitrate photolysis, based on observations of NO_x and HNO_3 collected onboard the NASA DC-8 aircraft during the KORUS-AQ field campaign. Using R_{obs} to evaluate HNO_3 production and loss, we demonstrate that the fastest proposed nitrate photolysis rates ($EF > 30$) are inconsistent with our current understanding of nitric acid production. Comparisons of the data from

KORUS-AQ with several other airborne observations show that the results from KORUS-AQ are not anomalous, and confirm that particle-phase nitrate photolysis is at most a minor HNO_3 loss pathway on a global scale.

Materials and Methods

Observations

The primary observations used in this analysis were taken onboard the NASA DC-8 as part of the Korea-United States Air Quality Study (KORUS-AQ) over South Korea during May and June 2016. Crucial observations used in this analysis include NO_x, gas-phase HNO_3, particle-phase nitrate, hydroxyl radical (OH), a wide range of volatile organic compounds (VOCs), and the spectrally-resolved actinic flux (used to calculate the gas-phase HNO_3 photolysis rate). Throughout the analysis, we use measurements of particle-phase nitrate from bulk aerosols collected onto filters and analyzed by ion chromatography. A full list of species used in this analysis and the techniques used to measure them are listed in Table 1. All analyses were performed using the merged dataset provided by NASA (version 4) of all KORUS-AQ flights, averaged to match the time resolution of the particle-phase nitrate filter measurements.

Additional data were obtained from the NASA LaRC Airborne Science Data for Atmospheric Composition website, from a set of six field deployments on the DC-8: INTEX-NA, MILAGRO, INTEX-B, ARCTAS-B, DC3, and SEAC4RS. A map of all 7 deployments is shown in Fig. S1. All of the campaigns include measurements of NO_x, HNO_3 in the gas and particle phase, $\Sigma RONO_2$, $\Sigma PANs$, and VOCs; all but one (SEAC4RS) include measurements of OH, although measurements of OH from INTEX-NA, MILAGRO, and INTEX-B include an interference from internally generated OH that can be important in some low-altitude environments.[22] NO on previous campaigns was always measured by chemiluminescence, but the instrument and group responsible was not consistent. On INTEX-NA, NO was measured

by the Brune group from Penn State, on INTEX-B by the Huey group from Georgia Tech, and on DC3 and SEAC4RS by the Ryerson group from NOAA ESRL.[23]

Table 1: Measurements from KORUS-AQ used in this analysis

Species	Technique	Principal Investigator	Reference
NO_2, $\Sigma RONO_2$, $\Sigma PANs$	TD-LIF[a]	R. Cohen	Day et al.[24]
NO, NO_y, O_3	Chemiluminescence	A. Weinheimer	Walega et al.[25]
HNO_3, gas-phase	CIMS[b]	P. Wennberg	Crounse et al.[26]
HNO_3, particle-phase	Filter-IC[c]	J. Dibb	Dibb et al.[27]
OH, HO_2	FAGE[d]	W. Brune	Faloona et al.[28]
VOCs	WAS-GC[e]	D. Blake	Blake et al.[29]
Oxygenated VOCs	PTR-MS[f]	A. Wisthaler	Wisthaler et al.[30]
HCHO	DFGAS [g]	A. Fried	Richter et al.[31]
CO, CH_4	TDLAS[h]	G. Diskin	Sachse et al.[32]
j_{gHNO_3}	Spectroradiometry	S. Hall	Shetter and Müller[33]

[a] Thermal Dissociation Laser-Induced Fluorescence; [b] Chemical-Ionization Mass Spectrometry; [c] Ion Chromatography; [d] Fluorescence Assay by Gas Expansion; [e] Whole Air Samples, followed by Gas Chromatography; [f] Proton Transfer Reaction Mass Spectrometry; [g] Difference Frequency Generation Absorption Spectroscopy; [h] Tunable Diode Laser Absorption Spectroscopy.

Airmass age and plume evolution

To distinguish between airmasses with fresh emissions and those that are highly aged, we use the ratio of 2-butyl nitrate to *n*-butane (2BN/nB) as a chemical clock.[34,35] 2-butyl nitrate has very few direct emissions, rather it is produced almost exclusively by the OH oxidation of *n*-butane and is lost by photolysis and oxidation. 2-butyl nitrate has a lifetime of weeks in the troposphere, compared to a lifetime of 1–2 days for *n*-butane.[36] The 2BN/nB ratio is therefore expected to increase monotonically with airmass age, and can be used to sort airmasses from the freshest emissions to the most highly aged.

Box Modeling

Box modeling was used in two ways to compare observations against predictions with different EFs. First, box modeling was used in a limited way to estimate the instantaneous production

and loss rates of NO_x and HNO_3 via routes that are not fully constrained from measurements. Secondly, a more comprehensive box model was used to study the evolution of advected plumes over the Yellow Sea. The framework and kinetics used for both applications are described here, while details specific to each application are described in their respective sections.

Simulations were run using the Framework for 0-Dimensional Atmospheric Modeling (F0AM), with chemical kinetics from the Master Chemical Mechanism v3.3.1 (MCM).[37,38] To include the uncertainty in many of the parameters, multiple simulations were run testing a range of values for each parameter. A full list of parameters specified or added to F0AM and their uncertainty ranges is included in Tables S1-S4 of the supplementary information.

Additional HNO_3 sources not included in the MCM were added to the model, including halogen chemistry, alkyl and multifunctional nitrate ($\Sigma RONO_2$) hydrolysis, and N_2O_5 hydrolysis. Inorganic halogen chemistry was added to the model following the scheme described in Sherwen et al.[39]. Total amounts of reactive chlorine, bromine, and iodine (Cl_y, Br_y, and I_y) were specified and allowed to partition freely between different halogen species. Total concentrations of Cl_y, Br_y, and I_y were set at 18 ppt, 3.5 ppt, and 5.5 ppt respectively, based on the modeled yearly average halogen concentrations over the Yellow Sea by Sherwen et al.[39].

Multiphase chemistry was added to the model through reactive uptake reactions onto a fixed aerosol surface area concentration. A reactive uptake parameter (γ) of 0.005 was applied to all $RONO_2$ with a tertiary nitrate group, equal to that assumed by Fisher et al.[40] for isoprene hydroxy nitrates. When using observed $\Sigma RONO_2$ concentrations, which are not isomer specific, a γ of 0.002 was applied to all nitrates. A γ of 0.10 was used for all three $XONO_2$ species, in between the laboratory values for uptake onto aqueous solution (0.03) and uptake onto sulfate aerosol (0.80).[41,42] A constant γ value of 0.014 was included for N_2O_5 chemistry.[43]

All the modeling studies were focused on plumes advected over the ocean, and therefore no

emissions were included in the model. Dilution was included as a first-order decay of model concentrations towards a prescribed background concentration, with an effective dilution rate of 1.7×10^{-5} s^{-1}. The average daytime boundary-layer deposition velocity for gas-phase HNO_3 used in the model is 2 cm s^{-1}.[44–46]

Results and Discussions

NO_x and HNO_3 chemistry during KORUS-AQ

Boundary layer measurements during KORUS-AQ typically observed high concentrations of HNO_3 and NO_x, although there was significant variation in the concentration of both species (Fig. 1). To gain greater sensitivity to the chemical loss processes of HNO_3, we restrict our analysis to observations in the boundary layer over the Yellow Sea. The air over the Yellow Sea was highly aged and contained high concentrations of NO_y, averaging 6 ± 2 ppb. Together, these properties result in slow chemical production of HNO_3 and emphasize the loss processes of HNO_3.

Boundary layer observations over the Yellow Sea are shown as the blue bars in Fig. 1. R_{obs} was typically extremely low, and was significantly lower than the ratios observed in the free troposphere (red bars in Fig. 1), indicating that boundary-layer chemistry, and not dilution, is controlling the ratio. The inorganic components of particles observed over the Yellow Sea were typically dominated by SO_4^{2-}, NH_4^+, and NO_3^- (Fig. S2a), although approximately a quarter of the filter samples showed enhanced concentrations of mineral ions (Fig. S2b).

FLEXPART back trajectories initialized from the points sampled by the DC-8 were used to further investigate the origin of the sampled air (Fig. S3).[47] The airmasses were often stagnant, showing slow circulation over the Yellow Sea, with the occasional rapid transport of air from China. Based on concentrations of CO_2 and black carbon, four of the samples appear to be influenced by nearby ship emissions and are excluded from further analysis.

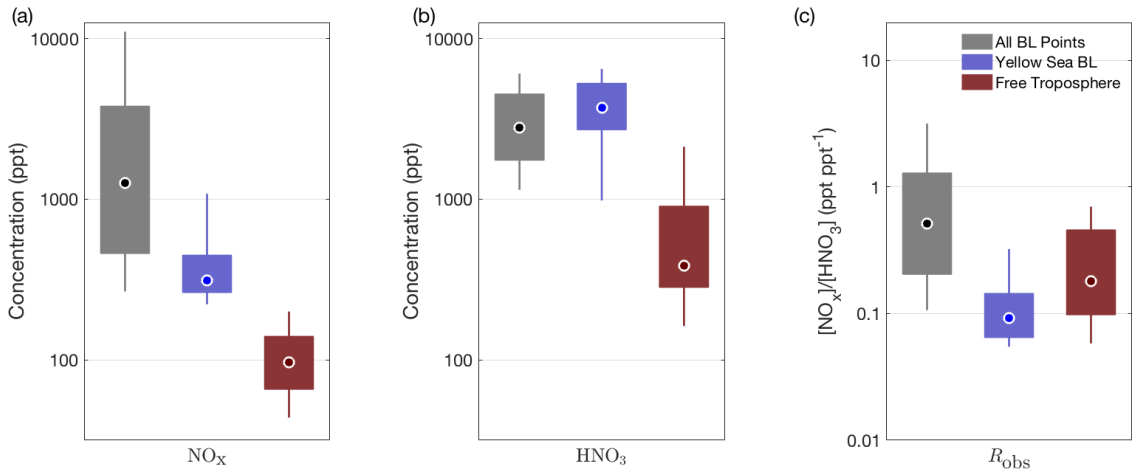

Figure 1: Distribution of NO_x, HNO_3 (gas + particle), and R_{obs} in three different regions during KORUS-AQ: all points in the boundary layer (gray bars), points in the boundary layer over the Yellow Sea (blue bars) and all points in the lower free troposphere (between 2 and 4 km, red bars). In each bar, the black dot shows the median value, the thick bar the inter-quartile range, and the thin line the 10^{th}-90^{th} percentiles.

To examine the compatibility of the observations with different proposed EFs, we compare R_{obs} with the calculated far-field ratios (R_{FF}), the predicted ratio of NO_x to HNO_3 in infinitely aged air. Because HNO_3 is not directly emitted to the atmosphere but is a product of NO_x oxidation, in an isolated plume R_{obs} starts at a maximum value and decreases to approach a far-field ratio set by the relative forward and backward conversion rates between NO_x and HNO_3. This behavior has been seen in past studies of NO_x chemistry in the outflow of plumes, which have found that R_{obs} decreases consistently as plumes evolves.[4,6,35,48,49] None of these studies observed an increase in R_{obs} with airmass age. Therefore, R_{obs} is expected to always be greater than or equal to R_{FF}.

Because R_{FF} represents the predicted NO_x/HNO_3 ratio in infinitely aged air, it is not directly observable. Although air in the free troposphere is typically highly aged, changes in chemistry with altitude prevent the NO_x/HNO_3 ratio in the free troposphere from being a useful proxy for R_{FF} in the boundary layer. Instead, R_{FF} is calculated algebraically from the effective first-order chemistry of NO_x, HNO_3, and PAN described by the system of differential equations (2)–(4). The eigenvector of the system with the largest associated eigenvalue gives

the predicted ratio of NO_x to HNO_3 in infinitely aged air.

$$\begin{aligned}
\frac{\mathrm{d}[\mathrm{NO_x}]}{\mathrm{d}t} &= -k_{\mathrm{forward}}[\mathrm{NO_x}] + k_{\mathrm{backward}}[\mathrm{HNO_3}] - k_{\mathrm{removal}}[\mathrm{NO_x}] \\
&\quad - k_{\mathrm{assoc}}[\mathrm{NO_x}] + k_{\mathrm{dissoc}}[\mathrm{PAN}] \qquad (2)\\
\frac{\mathrm{d}[\mathrm{HNO_3}]}{\mathrm{d}t} &= k_{\mathrm{forward}}[\mathrm{NO_x}] - k_{\mathrm{backward}}[\mathrm{HNO_3}] - k_{\mathrm{dep}}[\mathrm{HNO_3}] \qquad (3)\\
\frac{\mathrm{d}[\mathrm{PAN}]}{\mathrm{d}t} &= k_{\mathrm{assoc}}[\mathrm{NO_x}] - k_{\mathrm{dissoc}}[\mathrm{PAN}] \qquad (4)
\end{aligned}$$

The effective rate constants in these equations were calculated using observations from the DC-8, supplemented by box-modeling of unmeasured species. For each observation over the Yellow Sea, an independent box-model simulation was run to calculate the instantaneous concentration of RO_2 radicals and halogen nitrates. The partitioning of HNO_3 between gas and particle phases was set based on the observed concentrations of gas-phase nitric acid and particle-phase nitrate, and was assumed to remain constant as the plume evolved.

k_{forward}, the effective rate constant for conversion of NO_x into HNO_3, includes the oxidation of NO_2 by OH and the production of HNO_3 by $RONO_2$, $XONO_2$, and N_2O_5 hydrolysis. The backwards conversion rate, k_{backward}, includes contributions from gas-phase HNO_3 photolysis and oxidation and particle-phase photolysis. The loss of HNO_3 by deposition, k_{dep} was calculated using a deposition rate of 2 cm s^{-1} for gas-phase nitric acid only. k_{removal} represents the effects of NO_x removal through oxidation to $RONO_2$. k_{assoc} and k_{dissoc} are the effective first-order rate constants for the formation and dissociation of PAN respectively. Explicit formulas for these six effective first-order rate constants are given by Eq. S1–S6.

Figure 2 shows the ratio of ratios $R_{\mathrm{obs}}/R_{\mathrm{FF}}$ for several different values of the assumed EF. In addition to our best-guess estimates, Fig. 2 also shows sensitivity tests using high- and low-end estimates of halogen concentrations and HNO_3 deposition velocity, listed in Table S1. Because observed air masses may not yet have reached far-field conditions, $R_{\mathrm{obs}}/R_{\mathrm{FF}}$ is expected to always be greater than or equal to 1, setting an upper limit on the maximum

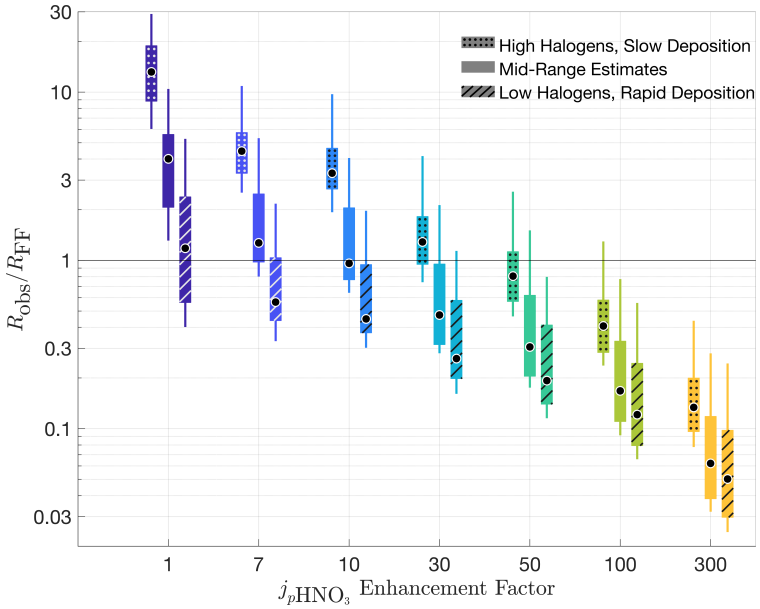

Figure 2: Comparison of R_{obs} to R_{FF} in the boundary layer over the Yellow Sea. Each individual bar shows a boxplot of the ratio of ratios, calculated using in-situ data for every observation over the Yellow Sea. For every value of EF tested, R_{FF} was calculated 3 different ways, using different assumptions for the production of nitric acid via halogen chemistry and the deposition velocity of nitric acid, corresponding to the range of values in Table S1. In each bar, the black dot shows the median value, the thick bar the inter-quartile range, and the thin line the 10^{th}-90^{th} percentiles. The boxplots are spaced equally and position along the x-axis does not correspond to EF on either a linear or a log scale.

EF compatible with the observations.

Although these values of R_{FF} are calculated from observations of plumes over the Yellow Sea, they are a reasonable approximation of what would be calculated in infinitely aged air. Fig. S5 in the supporting information shows the measured value of R_{obs} and the calculated value of R_{FF} in airmasses of different ages, using all boundary layer observations from KORUS-AQ. While R_{obs} decreases by 2 orders of magnitude between fresh emissions and highly aged air, R_{FF} remains roughly constant, further supporting for the conclusion that R_{obs}/R_{FF} should never be less than 1.

Using our best-guess estimates for the unknown parameters, an EF of up to 7 is consistent with the observations. With more generous assumptions, an EF of up to 30 is plausible. However, when an EF of 50 or greater is used, over 75% of the R_{FF}'s are greater than the

observed ratios and are therefore incompatible with the observations. Due to the extremely high values of R_{obs}/R_{FF} observed in fresh plumes, the analysis of Fig. 2 cannot be used to establish a lower limit on EF.

Box modeling of KORUS-AQ observations

To complement the analysis shown in Fig. 2, and to confirm that $R_{obs}/R_{FF} < 1$ could not be produced by changing chemistry in an evolving plume, we also ran a series of simulations examining the evolution of NO_y over the Yellow Sea. The effect of enhanced particle-phase HNO_3 photolysis was tested by comparing the results from simulation runs with seven different EFs: 1, 7, 10, 30, 50, 100, and 300. In all simulations, particle-phase HNO_3 photolysis was assumed to produce HONO in 100% yield, with no direct production of NO_x.

Due to significant uncertainties in many of the input parameters, random sampling was used to test the effects of different chemical parameters (Table S2), initial conditions (Table S3), and background concentrations (Table S4). Lacking detailed atmospheric measurements over China, we use as initial conditions the 5% of points observed during KORUS-AQ with the lowest 2BN/nB ratios. A random point from these observations was selected independently for each simulation, and the measured concentrations at that point were used as initial conditions for that run. Similarly, background concentrations were taken as a random sample from observations in the lower free troposphere (2–4 km) over the Yellow Sea. FLEXPART back trajectories of air in the lower free troposphere show that these airmasses were less likely to be stagnant than in the boundary layer, but typically originated in similar locations (Fig. S4). Gas-particle partitioning of HNO_3 was included as a fixed parameter that we varied based on the observations. For each simulation, a random value from the distribution of observed gas-particle partitionings was selected and assumed to remain constant for the model run. For parameters that were not measured (e.g. $[Br_y]$), a plausible range of values was constructed with the same best-guess estimate as used in the calculation of R_{FF}, and a random value from within that distribution was chosen independently for each simulation

run.

100 different simulations were run for each EF, and each simulation was run for five days. To ensure that the comparison of model results to observations is not biased by different airmasses ages, only a portion of each model simulation was included. To match the distribution of modeled and observed airmass ages, a random sample of 100 2BN/nB ratios was generated that matched the observed distribution of 2BN/nB over the Yellow Sea; then, for each of the model runs, only the timesteps with the modeled 2BN/nB ratios that most closely matched the random sample were selected. The sub-sampling procedure has only a minor effect on the results. Comparison of the observed distribution of 2BN/nB ratios with those calculated by the model in the first three days after initialization show reasonably good agreement, although model runs using the highest EFs result in air that is more aged than typically observed (Fig. S6). The sub-sample of each model run was further limited to daylight hours (solar zenith angle $\leq 45°$), to match the conditions when the DC-8 sampled air over the Yellow Sea.

The selected model points from each of the 100 different simulations for each EF were aggregated, and then compared with R_{obs} (Fig. 3a), as well as with concentrations of NO_x, HNO_3, ΣPANs, and OH (Fig. 3b–e). Model results and observations are presented as probability distributions, with the median highlighted as a circle (modeled) or a diamond (observed).

The model runs with the lowest EFs (1–10) are found to most closely reproduce R_{obs}. The overall spread in modeled R is greater than that observed over the Yellow Sea, suggesting that the range of input parameters is broader than that encountered in reality. The model runs with higher EFs (50–300) cannot reproduce values of R_{obs} of 0.06 or less, and at the highest EF values, many of the model runs predict R values of 0.3–1, values almost never observed over the Yellow Sea during KORUS-AQ. For a given EF, the spread in modeled NO_x to HNO_3 ratios was mostly explained by variation in parameters that controlled either the physical loss of HNO_3 or the gross production rate of HO_x radicals. This includes the

background concentration and deposition velocity of HNO_3, relative humidity, temperature, and background O_3 concentration.

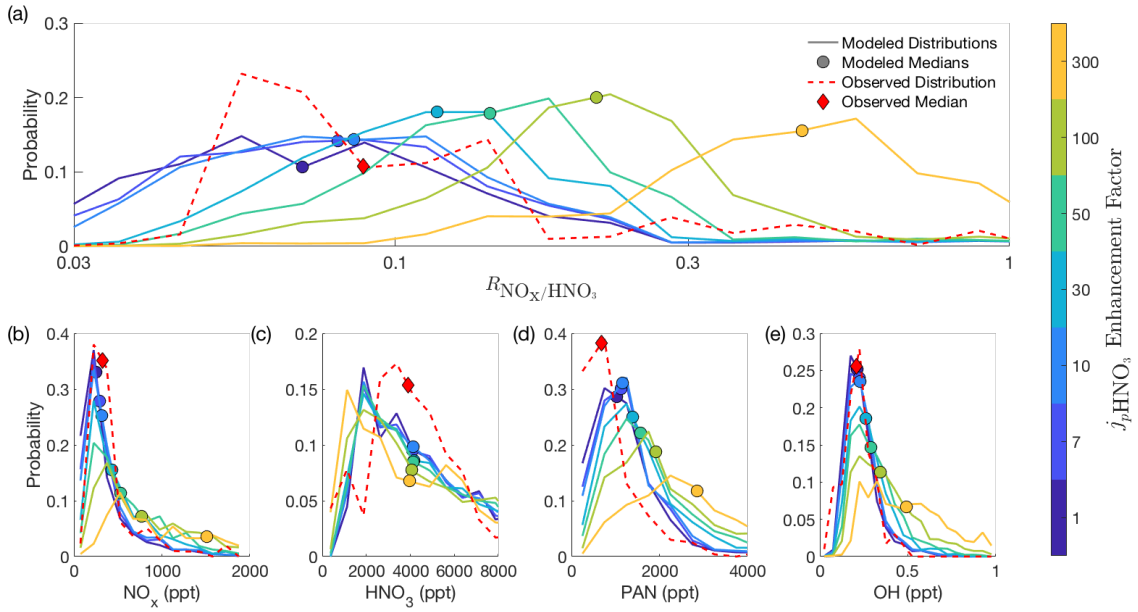

Figure 3: Probability distribution functions of R_{obs}, NO_x, HNO_3, ΣPANs, and OH from observations over the Yellow Sea and comparison with box model results using different assumed EFs.

Surprisingly, the increase in modeled R with increasing EF is not due to changes in the concentration of HNO_3 but instead is due to changes in NO_x (Fig. 3b–c). The median concentration of HNO_3 shows almost no change with increasing EF, indicating that the concentration of HNO_3 is controlled in large part by dilution and deposition rather than chemistry. The modeled distribution of HNO_3 is broader and peaks at a lower concentration than that observed, perhaps suggesting that the true deposition velocity for gas-phase HNO_3 is on the low-end of the range sampled by the model (1–4 cm s^{-1}). Wet deposition, not included in the model, also efficiently removes HNO_3 from the atmosphere and could potentially explain some of the observations with very low concentrations of HNO_3.

The modeled concentration of NO_x is much more sensitive to EF, likely reflecting the dominance of chemical processes to the NO_x budget. The model most closely reproduces the observed NO_x distribution at low EFs, but generally underestimates NO_x and overestimates

PAN (Fig. 3b,d). Higher EFs are also associated with greater concentrations of OH, due to increased HO_x cycling by NO (Fig. 3e). Production of HONO by nitrate photolysis also leads to production of HO_x radicals; however, the production of OH directly due to nitrate photolysis was less than 10% of HO_x production from O_3 and HCHO photolysis for all EFs.

Based on the results of Fig. 3, the observations over the Yellow Sea can be most accurately reproduced with low EFs, of 1–30. As the model does not take into account wet deposition or the effects of enhanced aerosol nitrate photolysis on background HNO_3 concentrations, an EF of 30 represents a likely upper limit to the true enhancement factor.

Comparison of KORUS-AQ to other measurements

To examine whether the results from KORUS-AQ are representative, the analysis of R_{obs}/R_{FF} was extended to six additional airborne campaigns conducted over the past 15 years on the NASA DC-8. In order to focus the analysis on airmasses where HNO_3 loss is most important, we only include observations of highly aged air, which we define as points with 2BN/nB greater than 0.06. The observations were further limited to the lowest 1.3 km above ground level.

Combined results from all seven campaigns are shown in Fig. 4. The top panel shows the distribution of R_{obs} found in highly aged air. The bottom panel extends the analysis of Fig. 2 and presents the results for the case where $EF = 10$ and using our best-guess assumptions about deposition and heterogeneous chemistry (Table S1). The same box-model calculations used in Fig. 2 were repeated for the six additional campaigns to estimate the concentration of halogen nitrates and RO_2 radicals. R_{FF} for SEAC4RS was calculated using a constant OH concentration of 0.18 ppt. The criteria used to select highly aged air in this section, chosen to ensure consistency among campaigns, are less restrictive than the ones applied to KORUS-AQ earlier in the paper and cause the values of R_{obs} and R_{obs}/R_{FF} reported in Fig. 4 to be higher than those reported in Fig. 2.

The results from KORUS-AQ are generally in line with those from other campaigns, al-

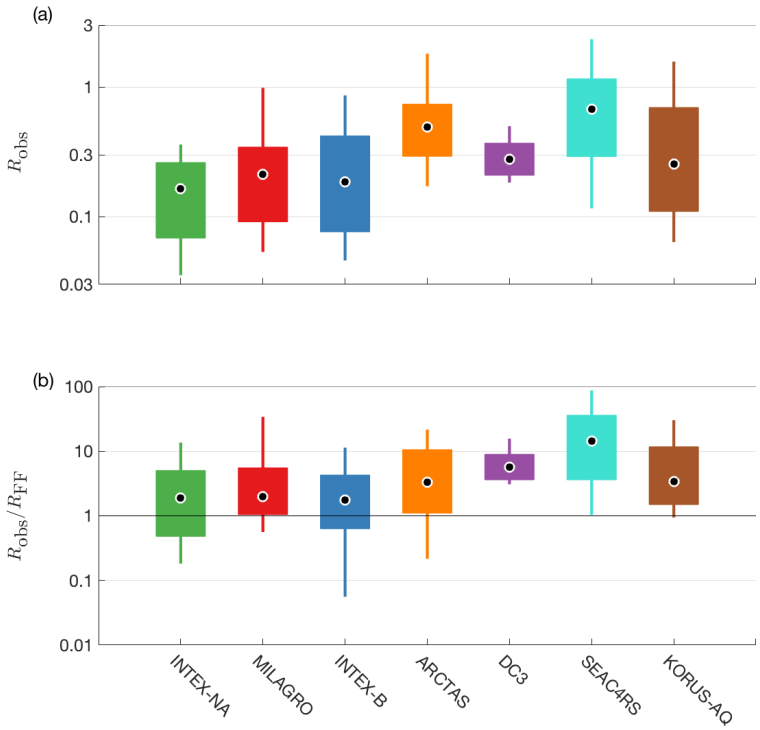

Figure 4: Analysis from KORUS-AQ extended to 6 additional campaign deployments. Panel (a) shows the observed far-field ratios of NO_x/HNO_3; Panel (b) shows the the ratio of ratios R_{obs}/R_{FF}, calculated assuming $EF = 10$ and $v_{dep,\ HNO_3} = 2$ cm s^{-1}.

though there is significant variation. One possible explanation for the variability in R_{obs}/R_{FF} is that there is variation in the rate of particulate nitrate photolysis between environments. Previous studies of HNO_3 photolysis on surfaces and in particles collected on filters have found significant variability in the reported photolysis rates, determined by, among other factors, the total concentration of particulate nitrate,[16] the presence of mineral dust aerosols,[50] and relative humidity.[50] However, observed values of R_{obs} in highly aged airmasses for all deployments do not show a significant trend with any of these three parameters (Fig. S7). But without direct measurements of the nitrate photolysis rate or HONO concentration, our power to find short periods of enhanced photolysis is limited.

Implications for HNO_3 and HONO

Based on eigenvector analysis of seven different airborne campaigns and detailed box modeling of plumes over the Yellow Sea, we have shown that observed values of NO_x and HNO_3 are consistent either with no enhanced aerosol nitrate photolysis, or with a relatively moderate enhancement factor. Using our best guess about the deposition velocity of HNO_3 and the contribution of unmeasured halogens to HNO_3 production, an enhancement factor of up to 10 is consistent with R_{obs} measured over the Yellow Sea. Using more generous assumptions for these parameters, an enhancement factor of up to 30 is consistent. Because these calculations compare observed NO_x to HNO_3 ratios with those predicted in infinitely aged air and do not take into account wet deposition, the EFs we calculate likely represent an upper limit to the compatible photolysis rate.

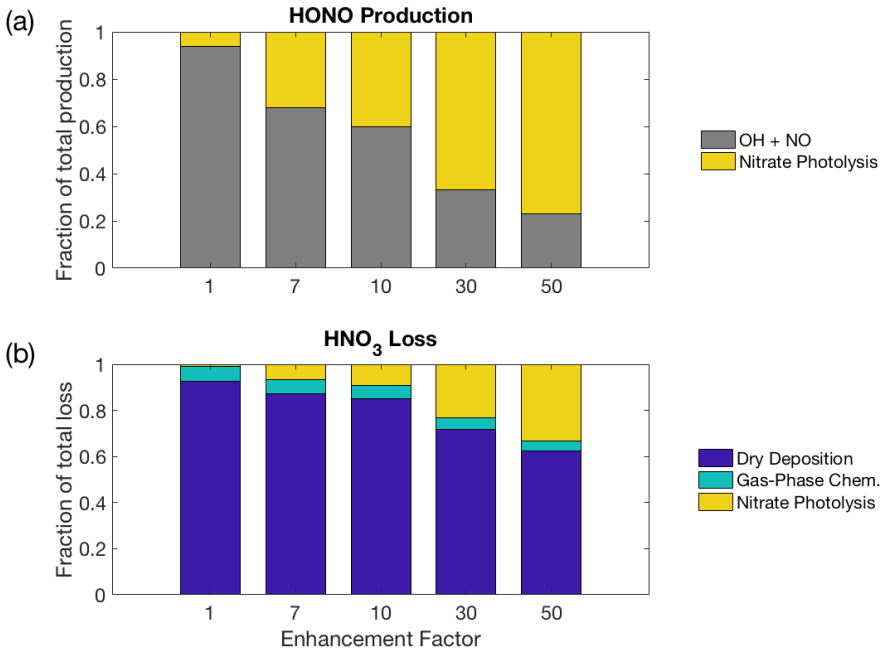

Figure 5: Effect of different particulate nitrate photolysis rates on the production of HONO (Panel a) and the loss of HNO_3 (Panel b), shown as a stacked bar graph. Each segment corresponds to the average fraction of total production or loss caused by a single pathway. Chemical rates were calculated using the average of all observations from all seven campaigns in the boundary layer in highly aged air, using the best-guess parameters in Table S1.

By turning aerosol nitrate into a source of NO_x, even relatively moderate EFs could

help resolve discrepancies between modeled and observed ratios of NO_x to HNO_3 in the remote atmosphere. Figure 5 shows the effect of different assumed EFs on the HONO and HNO_3 budgets. At $EF = 10$, nitrate photolysis would account for an average of 40% of total HONO production, but only 10% of HNO_3 loss, indicating that these rates of nitrate photolysis would have a much larger effect on HONO than on HNO_3.

Our result, arguing in favor of at most moderate enhancements in particle-phase nitrate photolysis, is compatible with multiple previous studies examining the chemistry of both HONO and NO_x. An average EF of 10–30 is less than our upper limit of EF and would be within the range found by Reed et al.[10] ($EF = 10$) and Kasibhatla et al.[12] ($EF = 25$–50) to best explain observations of HONO and NO_x at the Cape Verde Observatory.

However, there are also several studies that measured significantly higher rates of surface- and aerosol-phase nitric acid photolysis[13,16,21,51] as well as studies that postulated much higher rates of nitrate photolysis to explain observations of HONO.[11,14,15] Reconciling these observations with the present study would require either significant variability in the nitrate photolysis rate or additional sources of HONO. Laboratory studies have shown significant variability in the measured nitrate photolysis rate between samples as well as between populations of nitrate in the same sample.[16,51,52]

Alternatively, our calculation of R_{FF} could be missing an important oxidant that converts NO_x into HNO_3. Halogen concentrations are poorly constrained by current observations, and it is possible that total halogen concentrations could be much higher than typically assumed.[53] Halogen concentrations an order of magnitude larger than we assumed in our calculations could increase our maximum compatible EF from 30 up to 50. It is also possible that unknown oxidants represent a significant missing source of HNO_3 in the atmosphere.

Based on our observations of NO_x and HNO_3, we do not find evidence that particle-phase HNO_3 photolysis is extremely rapid, suggesting that if regional or global modeling studies include this pathway in their mechanisms, they should use an enhancement factor of 30 or less. On a global scale, nitrate photolysis is significantly slower than wet and dry

deposition, making re-noxification pathways at most a minor HNO_3 loss process. While enhancements of particle nitrate photolysis could help explain observations of HONO in the remote troposphere, the effects of nitrate photolysis on ozone and NO_x are likely to be smaller than proposed in some recent studies.

Acknowledgement

The authors thank NASA for support via NNX15AT85G (Berkeley), NNX15AT97G and NNX14AP46G (Caltech), NNX14AP46G (UNH) and NNX16AD96G (to Christoph Knote). Michelle J. Kim was supported by NSF AGS award 1524860. Methanol and acetaldehyde measurements were supported by the Austrian Federal Ministry for Transport, Innovation and Technology (bmvit) through the Austrian Research Promotion Agency (FFG). The authors thank Alan Fried for the formaldehyde measurements, Armin Wisthaler for the methanol and acetaldehyde measurements, Christoph Knote for the FLEXPART model results, Glenn Diskin for the CH_4 and CO measurements, and Andrew Weinheimer and Denise Montzka for NO measurements. We thank Tamara Sparks and Alex Teng for assistance in the field, the ground and flight crew of the DC-8, and the KORUS-AQ science team.

Supporting Information Available

The following files are available free of charge.

- `Nitrate_Photolysis_Supporting_Information.pdf`: Figures showing flight tracks, inorganic particle composition, FLEXPART back trajectories, evolution of R_{FF} with airmass age, modeled airmass age, and trends in R_{obs}; Tables listing all the parameters used in calculations of R_{FF} and in plume model; Equations with explicit formulas for effective rate constants used in the eigenvector analysis.

References

(1) Stavrakou, T.; Müller, J.-F.; Boersma, K. F.; van der A, R. J.; Kurokawa, J.; Ohara, T.; Zhang, Q. Key chemical NO_x sink uncertainties and how they influence top-down emissions of nitrogen oxides. *Atmos. Chem. Phys.* **2013**, *13*, 9057–9082, DOI: 10.5194/acp-13-9057-2013.

(2) Dulitz, K.; Amedro, D.; Dillon, T. J.; Pozzer, A.; Crowley, J. N. Temperature-(208–318 K) and pressure-(18–696 Torr) dependent rate coefficients for the reaction between OH and HNO_3. *Atmos. Chem. Phys.* **2018**, *18*, 2381–2394, DOI: 10.5194/acp-18-2381-2018.

(3) Pusede, S. E.; Duffey, K. C.; Shusterman, A. A.; Saleh, A.; Laughner, J. L.; Wooldridge, P. J.; Zhang, Q.; Parworth, C. L.; Kim, H.; Capps, S. L.; Valin, L. C.; Cappa, C. D.; Fried, A.; Walega, J.; Nowak, J. B.; Weinheimer, A. J.; Hoff, R. M.; Berkoff, T. A.; Beyersdorf, A. J.; Olson, J.; Crawford, J. H.; Cohen, R. C. On the effectiveness of nitrogen oxide reductions as a control over ammonium nitrate aerosol. *Atmos. Chem. Phys.* **2016**, *16*, 2575–2596, DOI: 10.5194/acp-16-2575-2016.

(4) Bertram, T. H.; Perring, A. E.; Wooldridge, P. J.; Crounse, J. D.; Kwan, A. J.; Wennberg, P. O.; Scheuer, E.; Dibb, J.; Avery, M.; Sachse, G.; Vay, S. A.; Crawford, J. H.; McNaughton, C. S.; Clarke, A.; Pickering, K. E.; Fuelberg, H.; Huey, G.; Blake, D. R.; Singh, H. B.; Hall, S. R.; Shetter, R. E.; Fried, A.; Heikes, B. G.; Cohen, R. C. Direct Measurements of the Convective Recycling of the Upper Troposphere. *Science* **2007**, *315*, 816–820, DOI: 10.1126/science.1134548.

(5) Neuman, J. A.; Parrish, D. D.; Trainer, M.; Ryerson, T. B.; Holloway, J. S.; Nowak, J. B.; Swanson, A.; Flocke, F.; Roberts, J. M.; Brown, S. S.; Stark, H.; Sommariva, R.; Stohl, A.; Peltier, R.; Weber, R.; Wollny, A. G.; Sueper, D. T.; Hubler, G.; Fehsenfeld, F. C. Reactive nitrogen transport and photochemistry in urban plumes

405 over the North Atlantic Ocean. *J. Geophys. Res. Atmos.* **2006**, *111*, D23S54, DOI:
406 10.1029/2005JD007010.

407 (6) Hauglustaine, D. A.; Ridley, B. A.; Solomon, S.; Hess, P. G.; Madronich, S. HNO_3/NO_x
408 ratio in the remote troposphere During MLOPEX 2: Evidence for nitric acid re-
409 duction on carbonaceous aerosols? *Geophys. Res. Lett.* **1996**, *23*, 2609–2612, DOI:
410 10.1029/96GL02474.

411 (7) Gao, R. S.; Fahey, D. W.; Del Negro, L. A.; Donnelly, S. G.; Keim, E. R.; Neuman, J. A.;
412 Teverovskaia, E.; Wennberg, P. O.; Hanisco, T. F.; Lanzendorf, E. J.; Proffitt, M. H.;
413 Margitan, J. J.; Wilson, J. C.; Elkins, J. W.; Stimpfle, R. M.; Cohen, R. C.; McEl-
414 roy, C. T.; Bui, T. P.; Salawitch, R. J.; Brown, S. S.; Ravishankara, A. R.; Port-
415 mann, R. W.; Ko, M. K. W.; Weisenstein, D. K.; Newman, P. A. A comparison of
416 observations and model simulations of NO_x/NO_y in the lower stratosphere. *Geophys.*
417 *Res. Lett.* **1999**, *26*, 1153–1156, DOI: 10.1029/1999GL900162.

418 (8) Perkins, K. K.; Hanisco, T. F.; Cohen, R. C.; Koch, L. C.; Stimpfle, R. M.; Voss, P. B.;
419 Bonne, G. P.; Lanzendorf, E. J.; Anderson, J. G.; Wennberg, P. O.; Gao, R. S.; Del Ne-
420 gro, L. A.; Salawitch, R. J.; McElroy, C. T.; Hintsa, E. J.; Loewenstein, M.; Bui, T. P.
421 The NO_x–HNO_3 System in the Lower Stratosphere: Insights from In Situ Measure-
422 ments and Implications of the J_{HNO_3}–[OH] Relationship. *J. Phys. Chem. A* **2001**, *105*,
423 1521–1534, DOI: 10.1021/jp002519n.

424 (9) Chatfield, R. B. Anomalous HNO_3/NO_x ratio of remote tropospheric air: Conversion
425 of nitric acid to formic acid and NO_x? *Geophys. Res. Lett.* **1994**, *21*, 2705–2708, DOI:
426 10.1029/94GL02659.

427 (10) Reed, C.; Evans, M. J.; Crilley, L. R.; Bloss, W. J.; Sherwen, T.; Read, K. A.; Lee, J. D.;
428 Carpenter, L. J. Evidence for renoxification in the tropical marine boundary layer.
429 *Atmos. Chem. Phys.* **2017**, *17*, 4081–4092, DOI: 10.5194/acp-17-4081-2017.

(11) Ye, C.; Heard, D. E.; Whalley, L. K. Evaluation of Novel Routes for NO_x Formation in Remote Regions. *Environ. Sci. Technol.* **2017**, *51*, 7442–7449, DOI: 10.1021/acs.est.6b06441.

(12) Kasibhatla, P.; Sherwen, T.; Evans, M. J.; Carpenter, L. J.; Reed, C.; Alexander, B.; Chen, Q.; Sulprizio, M. P.; Lee, J. D.; Read, K. A.; Bloss, W.; Crilley, L. R.; Keene, W. C.; Pszenny, A. A. P.; Hodzic, A. Global impact of nitrate photolysis in sea-salt aerosol on NO_x, OH, and O_3 in the marine boundary layer. *Atmos. Chem. Phys.* **2018**, *18*, 11185–11203, DOI: https://doi.org/10.5194/acp-18-11185-2018.

(13) Zhou, X.; Gao, H.; He, Y.; Huang, G.; Bertman, S. B.; Civerolo, K.; Schwab, J. Nitric acid photolysis on surfaces in low-NO_x environments: Significant atmospheric implications. *Geophys. Res. Lett.* **2003**, *30*, 2217, DOI: 10.1029/2003GL018620.

(14) Zhou, X.; Zhang, N.; TerAvest, M.; Tang, D.; Hou, J.; Bertman, S.; Alaghmand, M.; Shepson, P. B.; Carroll, M. A.; Griffith, S.; Dusanter, S.; Stevens, P. S. Nitric acid photolysis on forest canopy surface as a source for tropospheric nitrous acid. *Nat. Geosci.* **2011**, *4*, 440–443, DOI: 10.1038/ngeo1164.

(15) Ye, C.; Zhou, X.; Pu, D.; Stutz, J.; Festa, J.; Spolaor, M.; Tsai, C.; Cantrell, C.; Mauldin, R. L.; Campos, T.; Weinheimer, A.; Hornbrook, R. S.; Apel, E. C.; Guenther, A.; Kaser, L.; Yuan, B.; Karl, T.; Haggerty, J.; Hall, S.; Ullmann, K.; Smith, J. N.; Ortega, J.; Knote, C. Rapid cycling of reactive nitrogen in the marine boundary layer. *Nature* **2016**, *532*, 489–491, DOI: 10.1038/nature17195.

(16) Ye, C.; Zhang, N.; Gao, H.; Zhou, X. Photolysis of Particulate Nitrate as a Source of HONO and NO_x. *Environ. Sci. Technol.* **2017**, *51*, 6849–6856, DOI: 10.1021/acs.est.7b00387.

(17) Svoboda, O.; Kubelová, L.; Slavíček, P. Enabling Forbidden Processes: Quantum and

Solvation Enhancement of Nitrate Anion UV Absorption. *J. Phys. Chem. A* **2013**, *117*, 12868–12877, DOI: 10.1021/jp4098777.

(18) Warneck, P.; Wurzinger, C. Product quantum yields for the 305-nm photodecomposition of nitrate in aqueous solution. *J. Phys. Chem.* **1988**, *92*, 6278–6283, DOI: 10.1021/j100333a022.

(19) Nissenson, P.; Dabdub, D.; Das, R.; Maurino, V.; Minero, C.; Vione, D. Evidence of the water-cage effect on the photolysis of NO_3^- and $FeOH^{2+}$. Implications of this effect and of H_2O_2 surface accumulation on photochemistry at the air-water interface of atmospheric droplets. *Atmos. Environ.* **2010**, *44*, 4859–4866, DOI: 10.1016/j.atmosenv.2010.08.035.

(20) Zhu, C.; Xiang, B.; Zhu, L.; Cole, R. Determination of absorption cross sections of surface-adsorbed HNO_3 in the 290–330 nm region by Brewster angle cavity ring-down spectroscopy. *Chem. Phys. Lett.* **2008**, *458*, 373–377, DOI: 10.1016/j.cplett.2008.04.125.

(21) Zhu, C.; Xiang, B.; Chu, L. T.; Zhu, L. 308 nm Photolysis of Nitric Acid in the Gas Phase, on Aluminum Surfaces, and on Ice Films. *J. Phys. Chem. A* **2010**, *114*, 2561–2568, DOI: 10.1021/jp909867a.

(22) Mao, J.; Ren, X.; Zhang, L.; Van Duin, D. M.; Cohen, R. C.; Park, J.-H.; Goldstein, A. H.; Paulot, F.; Beaver, M. R.; Crounse, J. D.; Wennberg, P. O.; DiGangi, J. P.; Henry, S. B.; Keutsch, F. N.; Park, C.; Schade, G. W.; Wolfe, G. M.; Thornton, J. A.; Brune, W. H. Insights into hydroxyl measurements and atmospheric oxidation in a California forest. *Atmos. Chem. Phys.* **2012**, *12*, 8009–8020, DOI: 10.5194/acp-12-8009-2012.

(23) Ryerson, T. B.; Williams, E. J.; Fehsenfeld, F. C. An efficient photolysis system for

fast-response NO_2 measurements. *J. Geophys. Res.* **2000**, *105*, 26447–26461, DOI: 10.1029/2000JD900389.

(24) Day, D. A.; Wooldridge, P. J.; Dillon, M. B.; Thornton, J. A.; Cohen, R. C. A thermal dissociation laser-induced fluorescence instrument for in situ detection of NO_2, peroxy nitrates, alkyl nitrates, and HNO_3. *J. Geophys. Res.* **2002**, *107*, 4046, DOI: 10.1029/2001JD000779.

(25) Walega, J. G.; Dye, J. E.; Grahek, F. E.; Ridley, B. K. Compact measurement system for the simultaneous determination of NO, NO_2 , NOy, and O_3 using a small aircraft. Proc. SPIE 1433, Measurement of Atmospheric Gases. 1991; pp 232–241, DOI: 10.1117/12.46167.

(26) Crounse, J. D.; McKinney, K. A.; Kwan, A. J.; Wennberg, P. O. Measurement of Gas-Phase Hydroperoxides by Chemical Ionization Mass Spectrometry. *Anal. Chem.* **2006**, *78*, 6726–6732, DOI: 10.1021/ac0604235.

(27) Dibb, J. E.; Talbot, R. W.; Scheuer, E. M.; Blake, D. R.; Blake, N. J.; Gregory, G. L.; Sachse, G. W.; Thornton, D. C. Aerosol chemical composition and distribution during the Pacific Exploratory Mission (PEM) Tropics. *J. Geosphys. Res.* **1999**, *104*, 5785–5800, DOI: 10.1029/1998JD100001.

(28) Faloona, I. C.; Tan, D.; Lesher, R. L.; Hazen, N. L.; Frame, C. L.; Simpas, J. B.; Harder, H.; Martinez, M.; Di Carlo, P.; Ren, X.; Brune, W. H. A Laser-induced Fluorescence Instrument for Detecting Tropospheric OH and HO_2: Characteristics and Calibration. *J. Atmos. Chem.* **2004**, *47*, 139–167, DOI: 10.1023/B:JOCH.0000021036.53185.0e.

(29) Blake, N. J.; Blake, D. R.; Simpson, I. J.; Meinardi, S.; Swanson, A. L.; Lopez, J. P.; Katzenstein, A. S.; Barletta, B.; Shirai, T.; Atlas, E.; Sachse, G.; Avery, M.; Vay, S.; Fuelberg, H. E.; Kiley, C. M.; Kita, K.; Rowland, F. S. NMHCs and halocarbons in

Asian continental outflow during the Transport and Chemical Evolution over the Pacific (TRACE-P) Field Campaign: Comparison With PEM-West B. *J. Geophys. Res.* **2003**, *108*, 8806, DOI: 10.1029/2002JD003367.

(30) Wisthaler, A.; Hansel, A.; Dickerson, R. R.; Crutzen, P. J. Organic trace gas measurements by PTR-MS during INDOEX 1999. *J. Geophys. Res. Atmos.* **2002**, *107*, 8024, DOI: 10.1029/2001JD000576.

(31) Richter, D.; Weibring, P.; Walega, J. G.; Fried, A.; Spuler, S. M.; Taubman, M. S. Compact highly sensitive multi-species airborne mid-IR spectrometer. *Appl. Phys. B* **2015**, *119*, 119–131, DOI: 10.1007/s00340-015-6038-8.

(32) Sachse, G. W.; Hill, G. F.; Wade, L. O.; Perry, M. G. Fast-response, high-precision carbon monoxide sensor using a tunable diode laser absorption technique. *J. Geophys. Res. Atmos.* **1987**, *92*, 2071–2081, DOI: 10.1029/JD092iD02p02071.

(33) Shetter, R. E.; Müller, M. Photolysis frequency measurements using actinic flux spectroradiometry during the PEM-Tropics mission: Instrumentation description and some results. *J. Geophys. Res. Atmos.* **1999**, *104*, 5647–5661, DOI: 10.1029/98JD01381.

(34) Bertman, S. B.; Roberts, J. M.; Parrish, D. D.; Buhr, M. P.; Goldan, P. D.; Kuster, W. C.; Fehsenfeld, F. C.; Montzka, S. A.; Westberg, H. Evolution of alkyl nitrates with air mass age. *J. Geophys. Res.* **1995**, *100*, 22805–22813, DOI: 10.1029/95JD02030.

(35) Perring, A. E.; Bertram, T. H.; Farmer, D. K.; Wooldridge, P. J.; Dibb, J.; Blake, N. J.; Blake, D. R.; Singh, H. B.; Fuelberg, H.; Diskin, G.; Sachse, G.; Cohen, R. C. The production and persistence of $\Sigma RONO_2$ in the Mexico City plume. *Atmos. Chem. Phys.* **2010**, *10*, 7215–7229, DOI: 10.5194/acp-10-7215-2010.

(36) Clemitshaw, K. C.; Williams, J.; Rattigan, O. V.; Shallcross, D. E.; Law, K. S.; Cox, R. A. Gas-phase ultraviolet absorption cross-sections and atmospheric lifetimes

of several C_2–C_5 alkyl nitrates. *J. Photochem. Photobio. A* **1997**, *102*, 117–126, DOI: 10.1016/S1010-6030(96)04458-9.

(37) Wolfe, G. M.; Marvin, M. R.; Roberts, S. J.; Travis, K. R.; Liao, J. The Framework for 0-D Atmospheric Modeling (F0AM) v3.1. *Geosci. Model Dev.* **2016**, *9*, 3309–3319, DOI: 10.5194/gmd-9-3309-2016.

(38) Jenkin, M. E.; Young, J. C.; Rickard, A. R. The MCM v3.3.1 degradation scheme for isoprene. *Atmos. Chem. Phys.* **2015**, *15*, 11433–11459, DOI: 10.5194/acp-15-11433-2015.

(39) Sherwen, T.; Schmidt, J. A.; Evans, M. J.; Carpenter, L. J.; Großmann, K.; Eastham, S. D.; Jacob, D. J.; Dix, B.; Koenig, T. K.; Sinreich, R.; Ortega, I.; Volkamer, R.; Saiz-Lopez, A.; Prados-Roman, C.; Mahajan, A. S.; Ordóñez, C. Global impacts of tropospheric halogens (Cl, Br, I) on oxidants and composition in GEOS-Chem. *Atmos. Chem. Phys.* **2016**, *16*, 12239–12271, DOI: 10.5194/acp-16-12239-2016.

(40) Fisher, J. A.; Jacob, D. J.; Travis, K. R.; Kim, P. S.; Marais, E. A.; Chan Miller, C.; Yu, K.; Zhu, L.; Yantosca, R. M.; Sulprizio, M. P.; Mao, J.; Wennberg, P. O.; Crounse, J. D.; Teng, A. P.; Nguyen, T. B.; St. Clair, J. M.; Cohen, R. C.; Romer, P.; Nault, B. A.; Wooldridge, P. J.; Jimenez, J. L.; Campuzano-Jost, P.; Day, D. A.; Hu, W.; Shepson, P. B.; Xiong, F.; Blake, D. R.; Goldstein, A. H.; Misztal, P. K.; Hanisco, T. F.; Wolfe, G. M.; Ryerson, T. B.; Wisthaler, A.; Mikoviny, T. Organic nitrate chemistry and its implications for nitrogen budgets in an isoprene- and monoterpene-rich atmosphere: constraints from aircraft (SEAC^{4}RS) and ground-based (SOAS) observations in the Southeast US. *Atmos. Chem. Phys.* **2016**, *16*, 5969–5991, DOI: 10.5194/acp-16-5969-2016.

(41) Deiber, G.; George, Ch.; Le Calvé, S.; Schweitzer, F.; Mirabel, Ph. Uptake study of

552 $ClONO_2$ and $BrONO_2$ by Halide containing droplets. *Atmos. Chem. Phys.* **2004**, *4*,
553 1291–1299, DOI: 10.5194/acp-4-1291-2004.

554 (42) Hanson, D. R.; Ravishankara, A. R.; Lovejoy, E. R. Reaction of $BrONO_2$ with H_2O
555 on submicron sulfuric acid aerosol and the implications for the lower stratosphere. *J.*
556 *Geophys. Res.* **1996**, *101*, 9063–9069, DOI: 10.1029/96JD00347.

557 (43) McDuffie, E. E.; Fibiger, D. L.; Dubé, W. P.; Lopez-Hilfiker, F.; Lee, B. H.; Thorn-
558 ton, J. A.; Shah, V.; Jaeglé, L.; Guo, H.; Weber, R. J.; Reeves, J. M.; Weinheimer, A. J.;
559 Schroder, J. C.; Campuzano-Jost, P.; Jimenez, J. L.; Dibb, J. E.; Veres, P.; Ebben, C.;
560 Sparks, T. L.; Wooldridge, P. J.; Cohen, R. C.; Hornbrook, R. S.; Apel, E. C.; Cam-
561 pos, T.; Hall, S. R.; Ullmann, K.; Brown, S. S. Heterogeneous N_2O_5 Uptake During
562 Winter: Aircraft Measurements During the 2015 WINTER Campaign and Critical Eval-
563 uation of Current Parameterizations. *J. Geophys. Res. Atmos.* **2018**, *123*, 4345–4372,
564 DOI: 10.1002/2018JD028336.

565 (44) Ganzeveld, L.; Lelieveld, J. Dry deposition parameterization in a chemistry general cir-
566 culation model and its influence on the distribution of reactive trace gases. *J. Geophys.*
567 *Res.* **1995**, *100*, 20999–21012, DOI: 10.1029/95JD02266.

568 (45) Horii, C. V.; William Munger, J.; Wofsy, S. C.; Zahniser, M.; Nelson, D.;
569 Barry McManus, J. Atmospheric reactive nitrogen concentration and flux budgets
570 at a Northeastern U.S. forest site. *Agr. Forest Meteorol.* **2006**, *136*, 159–174, DOI:
571 10.1016/j.agrformet.2006.03.005.

572 (46) Nguyen, T. B.; Crounse, J. D.; Teng, A. P.; St. Clair, J. M.; Paulot, F.; Wolfe, G. M.;
573 Wennberg, P. O. Rapid deposition of oxidized biogenic compounds to a temperate forest.
574 *Proc. Natl. Acad. Sci. USA* **2015**, *112*, E392–E401, DOI: 10.1073/pnas.1418702112.

575 (47) Stohl, A.; Forster, C.; Frank, A.; Seibert, P.; Wotawa, G. Technical note: The La-

grangian particle dispersion model FLEXPART version 6.2. *Atmos. Chem. Phys.* **2005**, *5*, 2461–2474, DOI: 10.5194/acp-5-2461-2005.

(48) Pérez, I. M.; LaFranchi, B. W.; Cohen, R. C. Nitrogen oxide chemistry in an urban plume: investigation of the chemistry of peroxy and multifunctional organic nitrates with a Lagrangian model. *Atmos. Chem. Phys. Discuss.* **2009**, *9*, 27099–27165, DOI: 10.5194/acpd-9-27099-2009.

(49) Nault, B. A.; Garland, C.; Wooldridge, P. J.; Brune, W. H.; Campuzano-Jost, P.; Crounse, J. D.; Day, D. A.; Dibb, J.; Hall, S. R.; Huey, L. G.; Jimenez, J. L.; Liu, X.; Mao, J.; Mikoviny, T.; Peischl, J.; Pollack, I. B.; Ren, X.; Ryerson, T. B.; Scheuer, E.; Ullmann, K.; Wennberg, P. O.; Wisthaler, A.; Zhang, L.; Cohen, R. C. Observational Constraints on the Oxidation of NO_x in the Upper Troposphere. *J. Phys. Chem. A* **2016**, *120*, 1468–1478, DOI: 10.1021/acs.jpca.5b07824.

(50) Ndour, M.; Conchon, P.; D'Anna, B.; Ka, O.; George, C. Photochemistry of mineral dust surface as a potential atmospheric renoxification process. *Geophys. Res. Lett.* **2009**, *36*, L05816, DOI: 10.1029/2008GL036662.

(51) Baergen, A. M.; Donaldson, D. J. Photochemical Renoxification of Nitric Acid on Real Urban Grime. *Environ. Sci. Technol.* **2013**, *47*, 815–820, DOI: 10.1021/es3037862.

(52) Meusinger, C.; Berhanu, T. A.; Erbland, J.; Savarino, J.; Johnson, M. S. Laboratory study of nitrate photolysis in Antarctic snow. I. Observed quantum yield, domain of photolysis, and secondary chemistry. *J. Chem. Phys.* **2014**, *140*, 244305, DOI: 10.1063/1.4882898.

(53) Mahajan, A. S.; Oetjen, H.; Lee, J. D.; Saiz-Lopez, A.; McFiggans, G. B.; Plane, J. M. C. High bromine oxide concentrations in the semi-polluted boundary layer. *Atmos. Environ.* **2009**, *43*, 3811–3818, DOI: 10.1016/j.atmosenv.2009.05.033.

Graphical TOC Entry